RWKV-PCSSC: Exploring RWKV Model for Point Cloud Semantic Scene Completion

Wenzhe He*
Hunan University
College of Computer Science and
Electronic Engineering
Changsha, Hunan, China
hewenzhe@hnu.edu.cn

Hongyu Wang Hunan University College of Computer Science and Electronic Engineering Changsha, Hunan, China wanghongyu@hnu.edu.cn Xiaojun Chen*
Hunan University
College of Computer Science and
Electronic Engineering
Changsha, Hunan, China
chenxiaojun@hnu.edu.cn

Ying Liu[†]
Hunan Normal University
College of Information Science and
Engineering
Changsha, Hunan, China
liu_ying@hunnu.edu.cn

Wentang Chen Hunan University College of Computer Science and Electronic Engineering Changsha, Hunan, China B241000657@hnu.edu.cn

Ruihui Li[†]
Hunan University
College of Computer Science and
Electronic Engineering
Changsha, Hunan, China
liruihui@hnu.edu.cn

Abstract

Semantic Scene Completion (SSC) aims to generate a complete semantic scene from an incomplete input. Existing approaches often employ dense network architectures with a high parameter count, leading to increased model complexity and resource demands. To address these limitations, we propose RWKV-PCSSC, a lightweight point cloud semantic scene completion network inspired by the Receptance Weighted Key Value (RWKV) mechanism. Specifically, we introduce a RWKV Seed Generator (RWKV-SG) module that can aggregate features from a partial point cloud to produce a coarse point cloud with coarse features. Subsequently, the point-wise feature of the point cloud is progressively restored through multiple stages of the RWKV Point Deconvolution (RWKV-PD) modules. By leveraging a compact and efficient design, our method achieves a lightweight model representation. Experimental results demonstrate that RWKV-PCSSC reduces the parameter count by 4.18× and improves memory efficiency by 1.37× compared to state-of-the-art methods PointSSC[51]. Furthermore, our network achieves state-ofthe-art performance on established indoor (SSC-PC, NYUCAD-PC) and outdoor (PointSSC) scene dataset, as well as on our proposed datasets (NYUCAD-PC-V2, 3D-FRONT-PC).

CCS Concepts

• Applied computing \to Forecasting; • Computing methodologies \to Point-based models.

Keywords

Point Cloud, Semantic Scene Completion, RWKV

1 Introduction

Semantic scene completion (SSC) aims to generate a complete point cloud with accurate semantic labels from a partial point cloud input. SSC finds applications in domains such as autonomous driving and robotic navigation [13, 23, 38]. However, sensor limitations and

environmental complexities often lead to highly incomplete and noisy input data, posing significant challenges for scene completion and semantic interpretation.

SSCNet [33] first proposed the use of voxel-based methods to address the SSC task, and since then, many subsequent works [13, 21, 23, 25, 38, 42] have adopted voxel-based approaches for SSC. Voxel representation necessitates the discretization of 3D space, resulting in the generation of a large number of voxel units. As resolution increases, the computational and storage demands also increase significantly, leading to high computational costs.

Considering the limitations of voxel representation [50, 58], methods such as PCSSC-Net [58] have been proposed to address these challenges. Specifically, PCSSC-Net uses a 12-dimensional feature vector, which includes point coordinates, RGB values, normal vectors, and differential coordinates, as input to the network to generate a complete segmented point cloud. Although PCSSC-Net has yielded promising results, they do not adequately account for the important relationship between scene completion and semantic segmentation. CasFusionNet [50] aims to achieve dense feature fusion between the two tasks, demonstrating commendable performance. However, it directly downsamples the input to generate coarse point clouds, which oversimplifies the task, fails to predict missing regions, and loses geometric information. PointSSC [51] has demonstrated promising performance on its proposed outdoor scene dataset. However, it fails to capture the point cloud's intricate features fully. Furthermore, both PointSSC and CasFusionNet suffer from complex architectures, resulting in a large number of parameters and significant memory usage.

The latest advancements in the RWKV model for Natural Language Processing (NLP) demonstrate its efficiency in handling global information and sparse inputs. Building on these strengths, we propose a novel method for semantic scene completion, termed RWKV-PCSSC, which initially integrates an RWKV seed generator (RWKV-SG) module to construct a coarse point cloud enriched with point-wise features. These features are subsequently refined through multiple RWKV Point Deconvolution (RWKV-PD) module stages. RWKV-PD enables iterative refinement and segmentation

^{*}Both authors contributed equally to this research.

[†]Corresponding authors

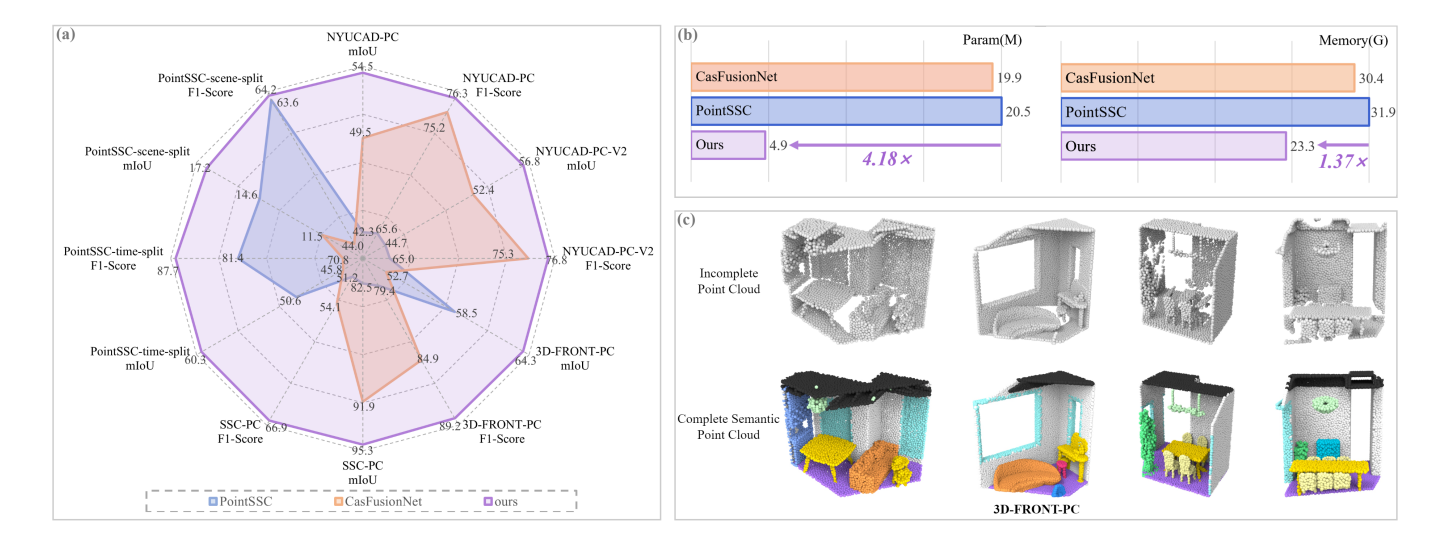


Figure 1: (a) Compared to CasFusionNet [50] and PointSSC [51], RWKV-PCSSC achieves state-of-the-art performance in both scene completion and segmentation across a variety of indoor and outdoor datasets. (b) On PointSSC datasets, RWKV-PCSSC significantly reduces parameters and memory usage while maintaining competitive performance. (c) We introduce 3D-FRONT-PC, a novel semantic scene completion dataset derived from 3D-FRONT [9, 10] scene models. Compared to NYUCAD-PC, 3D-FRONT-PC presents more challenging tasks (i.e., retaining input point cloud coordinates in the world coordinate system), covers more categories (i.e., increased from 11 to 20), and scales significantly larger (i.e., expanded from 1,449 to 12,655 instances).

of the coarse point cloud to progressively achieve precise scene completion and segmentation.

Currently, research on point cloud semantic scene completion (PCSSC) remains relatively limited, partly due to the scarcity of relevant datasets. Therefore, To address this shortfall, we introduce 3D-FRONT-PC, a novel dataset derived from 3D-FRONT scene models. Compared to the NYUCAD-PC dataset, 3D-FRONT-PC presents three major challenges. First, it requires preserving input point cloud coordinates in the world coordinate system. Second, the category range is expanded from 11 to 20 classes. Third, the dataset size is significantly increased from 1,449 to 12,655 instances. Additionally, we propose NYUCAD-PC-V2, an enhanced iteration of NYUCAD-PC that resolves semantic ambiguities present in the original dataset. To validate the effetiveness of our method, we evaluated RWKV-PCSSC on four indoor datasets: 3D-FRONT-PC, NYUCAD-PC-V2, NYUCAD-PC [8, 50], and SSC-PC [58], as well as on the outdoor dataset PointSSC [51] with its two data division strategies, split by time and split by scene. Our network performed excellently well in quantitative and qualitative experiments, significantly outperforming existing state-of-the-art methods. Figure 1 (a) compares our method with others in terms of segmentation and completion performance. In the indoor datasets SSC-PC [23], NYUCAD-PC [50], NYUCAD-PC-V2, and 3D-FRONT-PC, as well as the outdoor datasets PointSSC-scene-split and PointSSC-timesplit [51], our approach consistently achieves state-of-the-art performance in both segmentation and completion metrics. Furthermore, Figure 1 (b) compared to the state-of-the-art method [51] on PointSSC [51] dataset, our approach achieves a 76.1% reduction in parameter count and a 27.0% reduction in memory usage. This research not only provides a new perspective for semantic scene completion but also offers robust support for related fields of study. In conclusion, the contributions of our paper can be summarized as follows:

- RWKV-PCSSC achieves state-of-the-art performance in point cloud semantic scene completion across diverse datasets, outperforming PointSSC [51] with 76.1% fewer parameters and 27.0% less memory.
- We designed two novel modules: the RWKV seed generator (RWKV-SG) module to generate an initial coarse point cloud with point-wise features, which is iteratively refined and segmented through the RWKV Point Deconvolution (RWKV-PD) module for precise point cloud completion and segmentation.
- We present two datasets: 3D-FRONT-PC, which comprises 12,655 point cloud scene with 20 label categories derived from the 3D-FRONT[9, 10] dataset, and NYUCAD-PC-V2, an enhanced version of NYUCAD-PC[8, 50] that addresses semantic ambiguities in the original dataset.

2 Related Work

Point Cloud Segmentation. PointNet [29] and PointNet++ [30] pioneered point-based networks using Set Abstraction to model point relationships. Subsequent works [2, 26, 31, 35, 36, 43] advanced segmentation by addressing fine-grained geometric and contextual challenges in large-scale 3D environments. Attention-based methods [2, 11, 18, 37, 47, 48, 60] demonstrated superior performance by effectively handling the permutational invariance of point clouds. Mamba-based approaches [14, 22, 59] have shown improved scalability and efficiency compared to transformers.

Point Cloud Completion. PCN [56] pioneered completion by learning latent shape representations to generate missing points.

Subsequent methods [24, 32, 34, 46, 55, 61, 62] have been proposed to advance point cloud completion, significantly improving robustness and accuracy. SnowflakeNet [49] introduced a snowflake-like growth process for point generation. PointAttN [40] employs attention mechanisms to model local geometric relationships, demonstrating significant performance.

Receptance Weighted Key Value (RWKV) [28]. The Receptance Weighted Key Value (RWKV) model integrates the parallel training efficiency of transformers with the linear computational scalability of RNNs, offering a compelling solution for sequence processing tasks. By utilizing a redesigned linear attention mechanism, RWKV overcomes the quadratic scaling limitations inherent in traditional Transformers, making it particularly well-suited for long-sequence reasoning. Furthermore, its successful adaptation to visual domains [6, 7, 15, 41, 53], exemplifies its versatility. for instance, Vision-RWKV [6] has been implemented for high-resolution image processing, while PointRWKV [15] facilitates effective 3D point cloud encoding. These adaptations underscore the model's efficiency and broad applicability in complex tasks, including advanced 3D spatial analysis.

Semantic Scene Completion. Existing segmentation and completion methods often neglect the interdependencies between these tasks, leading to suboptimal results due to their inherent complementarity. Semantic scene completion (SSC) has emerged as a pivotal task in 3D computer vision, aiming to generate complete and semantically annotated 3D scenes from partial observations. Recent studies [1, 21, 25, 39, 42] predominantly adopt voxel-based representations, discretizing incomplete scenes into 3D voxel grids. These grids are processed using 3D Convolutional Neural Networks (3D CNNs), which excel at capturing spatial context and local dependencies. For example, SSCNet [33] pioneered SSC by employing an end-to-end 3D convolutional network. Subsequent works [20, 57] improved voxel-based modeling through modified 3D convolutions, while [19] introduced instance-level completion by deforming templates with latent codes. Additionally, recent advancements [3, 4, 25] integrate depth and color features into 2D semantic networks, further enhancing performance.

Point Cloud Semantic Scene Completion. Although voxelbased methods enable effective volumetric data processing, they often incur high computational costs due to excessive parameters and voxel grid memory overhead. In contrast, point clouds provide a more memory-efficient and flexible representation of 3D data, capturing intricate geometric details while avoiding the resolution limitations inherent in voxel-based methods. SSCPC-Net [58] addresses semantic scene completion using a 12-dimensional feature vector as input and designing a patch-based contextual encoder to predict a completed and segmented point cloud. Recently, CasFusionNet [50] attempted to bridge this gap by promoting feature exchange between the completion and segmentation modules, thus improving the interaction between these tasks. PointSSC [51] achieves efficient and accurate semantic scene completion by effectively integrating global and local features for large-scale outdoor environments. However, these methods are often limited by their complex and cumbersome architecture, leading to an overabundance of parameters and considerable memory usage, which hinders their practical scalability. Moreover, they demonstrate constrained capability in

effectively capturing both geometric structures and semantic correlations, resulting in suboptimal performance for semantic scene completion tasks. In this paper, we propose RWKV-PCSSC, a novel point cloud semantic scene completion network that leverages the RWKV mechanism to enhance parameter efficiency and accuracy.

3 Method

3.1 Overview Pipeline

Given an incomplete point cloud $P_{in} \in \mathbb{R}^{N \times 3}$ containing N points as input, our goal is to produce a complete 3D scene $P_{out} \in \mathbb{R}^{M \times 3}$ with M points ($M \geq N$), along with the predicted per-point semantic labels $L_{out} \in \mathbb{R}^{M \times C}$, where C denotes the total number of semantic classes. Figure 2 (a) illustrates the overall structure of RWKV-SSCPC: The network first produces coarse features alongside a semantically labeled coarse point cloud via the RWKV-SG module, followed by multiple stages of RWKV-PD modules that refine the output in a coarse-to-fine manner [32, 40, 44, 45, 61] to produce a completed and segmented point cloud. Below, we elaborate on the steps in our pipeline.

First, we input P_{in} into the RWKV-SG module, which generates a coarse point cloud with semantic labels, denoted as P_{coarse} and L_{coarse} . Relying solely on P_{coarse} as inputs for the next stage of the RWKV-PD module can lead to the loss of details within the input point cloud data, which would negatively impact the overall refinement process. To fully leverage the features of the input point cloud, our RWKV-SG module also outputs the point-wise feature F_{coarse} of the coarse point cloud. We then use P_{coarse} and F_{coarse} as inputs to the first RWKV-PD module. Specifically, P_{coarse} and F_{coarse} correspond to P_{i-1} , F_{i-1} of the first RWKV-PD module, respectively. Throughout the N stages of refinement, for example, in the i-th stage $(2 \le i \le N)$, the RWKV-PD inputs consist of the outputs from the previous RWKV-PD stage. In the initial RWKV-PD stage (i = 1), the input to RWKV-PD is sourced from the output of the preceding RWKV-SG. This hierarchical coarse-to-fine approach progressively reconstructs the point-wise features of the point cloud, ultimately yielding a fully complete segmented point cloud P_{out} and L_{out} .

3.2 RWKV Seed Generator

Although several studies have addressed semantic scene completion tasks in point clouds, existing methods remain limited in their ability to predict detailed geometries for missing regions and effectively capture local structural information during coarse point cloud generation. To overcome these limitations, the RWKV Seed Generator (RWKV-SG) module was developed. This module extracts essential local and global geometric features from the input point cloud to predict and reconstruct missing regions, generates a coarse point cloud P_{coarse} with corresponding semantic labels L_{coarse} , and produces detailed point-wise features F_{coarse} , thereby furnishing adequate information for subsequent RWKV-PD modules. Figure 2 (b) illustrates the detailed architecture of RWKV-SG.

We first employ the PointNet module [30] to extract preliminary features from the input point cloud P_{in} . Subsequently, to further explore the deep-level features within the point cloud data, we introduce the PRWKV module. Leveraging its robust sequence modeling capabilities, the PRWKV module enhances and abstracts the preliminary features across multiple levels (i.e., M=4 as illustrated

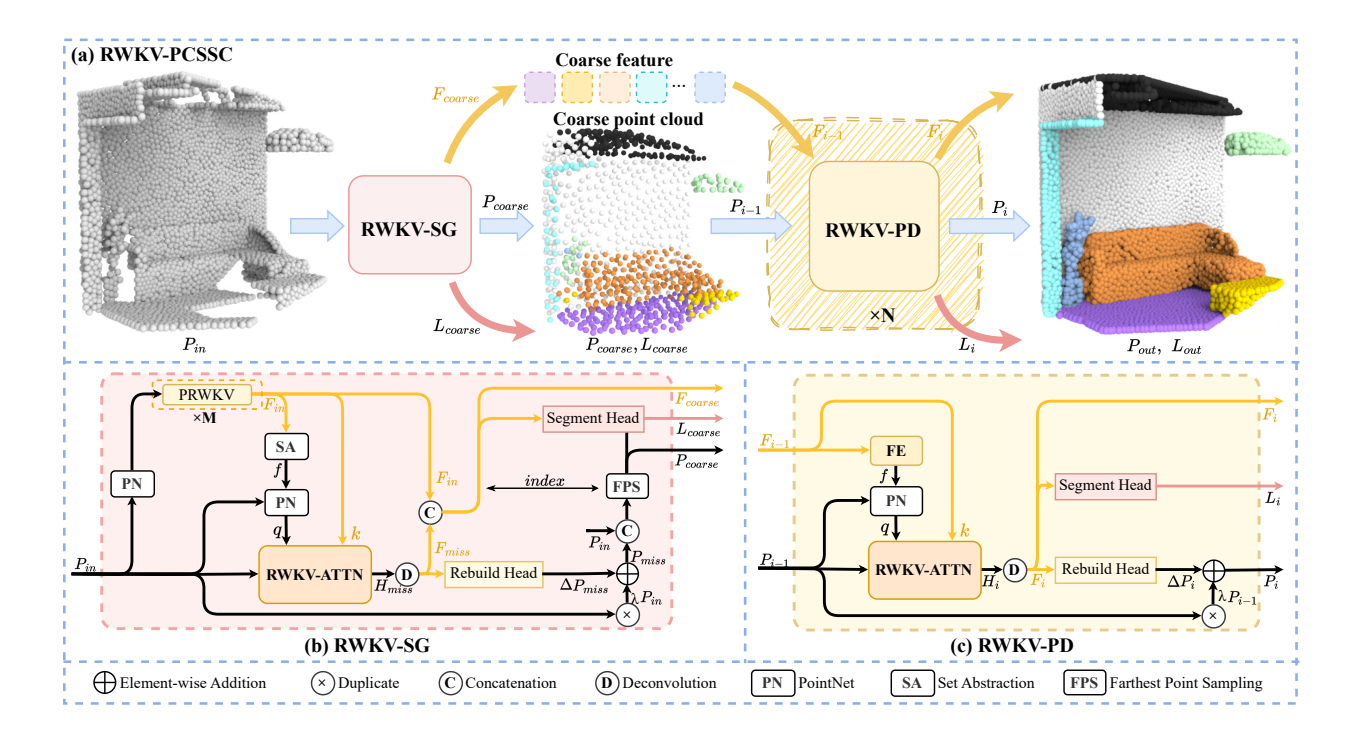


Figure 2: (a) The architecture of the RWKV-PCSSC network is depicted as follows. The network comprises an RWKV Seed Generator (RWKV-SG) module and a sequence of N stages, each consisting of RWKV Point Deconvolution (RWKV-PD) modules. (b) Detailed description of the RWKV-SG module. (c) The details of the RWKV-PD module.

in Figure 2 (b)), thereby obtaining more discriminative high-order feature representations F_{in} . Next, we utilize the Set Abstraction module [30] to extract the global feature f. The global feature f is then combined with P_{in} and fed into the PointNet module to obtain the query q_{in} . Subsequently, F_{in} is treated as k_{in} , P_{in} , q_{in} , k_{in} and input into the RWKV-ATTN module to predict hidden information about missing parts, denoted as H_{miss} . Subsequently, H_{miss} is passed into the Deconvolution module to obtain F_{miss} . To derive ΔP , we employ an MLP with a tanh activation function as our Rebuild Head. ΔP is then added to P_{in} to obtain P_{miss} . To generate the complete coarse point cloud P_{coarse} , we apply farthest point sampling (FPS) to the concatenation of P_{in} and P_{miss} , while simultaneously obtaining its corresponding feature F_{coarse} . Finally, we process F_{coarse} using a Segment Head composed of KPConvD [37], PRWKV and MLP to obtain the semantic labels L_{coarse} .

The final outputs of the RWKV-SG: P_{coarse} , F_{coarse} , are propagated as hierarchical inputs to the first stage RWKV-PD module for progressive refinement.

3.3 RWKV Point Deconvolution

The purpose of RWKV Point Deconvolution (RWKV-PD) is to progressively refine the coarse point cloud P_{coarse} into a complete point cloud with semantic labels. Figure 2 (c) shows the detailed architecture of our designed RWKV-PD.

Notably, the input for the first stage of RWKV-PD(i=1) in the network is derived from the preceding RWKV-SG module, while the input for each subsequent stage($2 \le i \le N$) originates from

the output of the RWKV-PD module in the previous stage. We first use the Feature Extractor to extract the global feature f from F_{i-1} , and the same Feature Extractor is applied at each stage to extract the relevant hierarchical features. The Feature Extractor consists of PRWKV and the Set Abstraction module. This approach ensures consistency in feature representation. Subsequent to feature extraction, P_{i-1} and f are further processed through a PointNet module [29] to obtain q_i . We set F_{i-1} as k_i , and input P_{i-1} , q_i , k_i into the RWKV-ATTN to obtain the hidden feature H_i . Subsequently, the hidden feature H_i is passed through the deconvolution module [49] to derive F_i . Finally, F_i is processed by the Rebuild Head and the Segment Head to obtain a displacement vector ΔP and the updated semantic label L_i , respectively. The previous position P_{i-1} is then replicated λ times, and the displacement ΔP is added to it, resulting in the updated position P_i .

3.4 RWKV Attention (RWKV-ATTN)

The structure of the RWKV-ATTN module is illustrated in Figure 3 (a). Leveraging the efficient global modeling capability of PRWKV and local attention mechanisms, the proposed RWKV-ATTN module more effectively learns abstract features between parent points and their corresponding child points.

For computing the value v, the query q and key k are first concatenated and passed through an MLP to obtain v. The vector v is fed into two PRWKV modules, and the final value feature \hat{v} is derived through a gating mechanism, which adaptively controls the global information flow and enhances feature selectivity, as

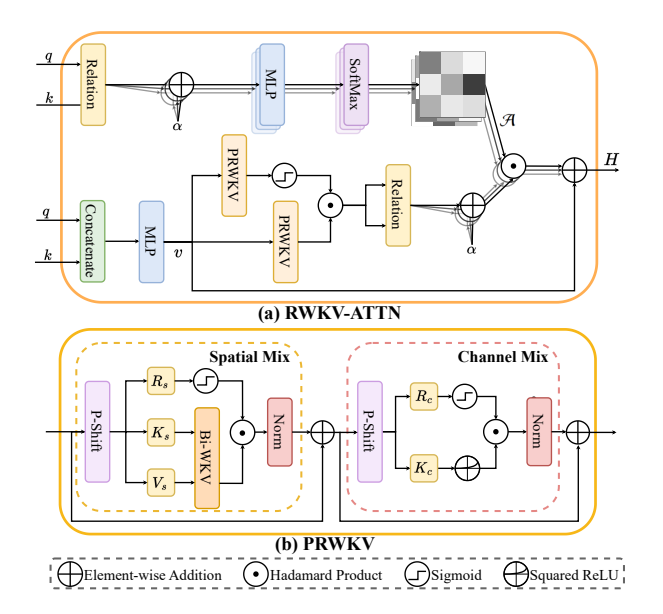


Figure 3: (a) The detailed architecture of the RWKV-ATTN. (b) The detailed architecture of the PRWKV.

formulated below:

$$\hat{v} = \sigma(PRWKV(v)) \odot PRWKV(v), \tag{1}$$

where σ is the Sigmoid function, \odot is Hadamard Product.

For computing attention weights, the RWKV-ATTN module employs subtraction relation in a local neighborhood L(i) (k-nearest neighbors) to calculate local relationships between query q and key k. These local relationships are then combined with positional encoding α , processed through MLP and SoftMax function to generate the final attention weights $\mathcal A$. Specifically, $\mathcal A$ can be calculated as

$$\mathcal{A} = \frac{exp(MLP(q_i - k_j + \alpha))}{\sum_{j \in L(i)} exp(MLP(q_i - k_j + \alpha))}, j \in L(i). \tag{2}$$

After obtaining the value \hat{v} and the attention weights \mathcal{A} , we perform an element-wise multiplication (Hadamard product) between them and then add the intermediate value v obtained from the MLP. This process can be formally expressed as:

$$H = \mathcal{A} \odot \left(\sum_{j \in L(i)} (\hat{v}_i - \hat{v}_j + \alpha) \right) + v, j \in L(i). \tag{3}$$

This operation leverages the efficient global feature capture of PRWKV alongside local attention mechanisms to extract local features, improving the expressiveness of the hidden features H.

3.5 Point RWKV (PRWKV)

An overview of our PRWKV is depicted in Figure 3 (b). PRWKV is designed to efficiently process point clouds by integrating two key components: a spatial-mix module and a channel-mix module. The spatial-mix module functions as an attention mechanism, performing linear complexity global attention computation to capture long-range dependencies within the point cloud. This module is crucial for capturing the global structure of the point cloud. The

channel-mix module serves as a feedforward network (FFN), performing feature fusion in the channel dimension to enhance the representation of local features. This dual-module design allows PRWKV to balance global context modeling and local detail preservation effectively.

In the Spatial Mixing module, input features are processed through a shift operation, referred to as P-Shift, as illustrated in Figure 4. Unlike images or voxels, point clouds are inherently unordered. To perform the shift operation on point clouds, we first serialize them. Specifically, whenever a new point cloud is introduced, we randomly apply one of the following serialization methods: z-order [27], Hilbert-order [16]. This serialization transforms the unordered point cloud into an ordered sequence, enabling the P-Shift operation. The P-Shift operation is formally defined as:

$$P-\text{Shift}_{(*)}(X) = X + (1 - \mu_{(*)})X',$$

$$X' = \text{Concat}(X_1, X_2, X_3, X_4),$$
(4)

where $(*) \in \{R, K, V\}$ denotes the interpolation of X and X', controlled by the learnable vectors $\mu_{(*)}$.

In *P*-Shift, the complete point cloud sequence with *n* points is uniformly divided into *s* subsequences, each containing n/s points. Thus, X' represents the slicing vector of X, defined as:X, i.e., $X_1 = [s, n/s - 1, 0 : C/4]$, $X_2 = [s, n/s + 1, C/4 : C/2]$, $X_3 = [s, n/s - 1, C/2 : 3C/4]$, $X_4 = [s, n/s + 1, 3C/4 : C]$. The *P-Shift* function enhances the attention mechanism by enabling it to focus on proximate points across diverse channels without significantly increasing computational overhead. This process further broadens the receptive field, thereby enhancing the point coverage in subsequent layers. The process of *P-Shift* is shown in Figure 4.

After P-Shift, the features projected into matrices R_s , K_s , and $V_s \in \mathbb{R}^{T \times C}$ via parallel linear transformations:

$$R_{s} = P-Shift_{R}(X)W_{R},$$

$$K_{s} = P-Shift_{K}(X)W_{K},$$

$$V_{s} = P-Shift_{V}(X)W_{V}.$$
(5)

The global attention output **wkv** is computed via a linear-complexity bidirectional attention mechanism Bi-WKV [5], applied to K_s and V_s to enhance contextual modeling:

$$wkv = Bi - WKV(K_s, V_s). (6)$$

The attention result for the *t*-th feature token is given by:

$$wkv_t = Bi\text{-}WKV(K,V)_t. \frac{\sum_{i=0,i\neq t}^{T-1} e^{-(|t-i|-1)/T\cdot\omega + k_i} v_i + e^{u+k_t} v_t}{\sum_{i=0}^{T-1} e^{-(|t-i|-1)/T\cdot\omega + k_i} + e^{u+k_t}}. \tag{7}$$

The output O_s is obtained by element-wise multiplication of $\sigma(R_s)$ and wkv, followed by a linear projection and layer normalization:

$$O_s = LayerNorm\left((\sigma(R_s) \odot wkv)W_O\right).$$
 (8)

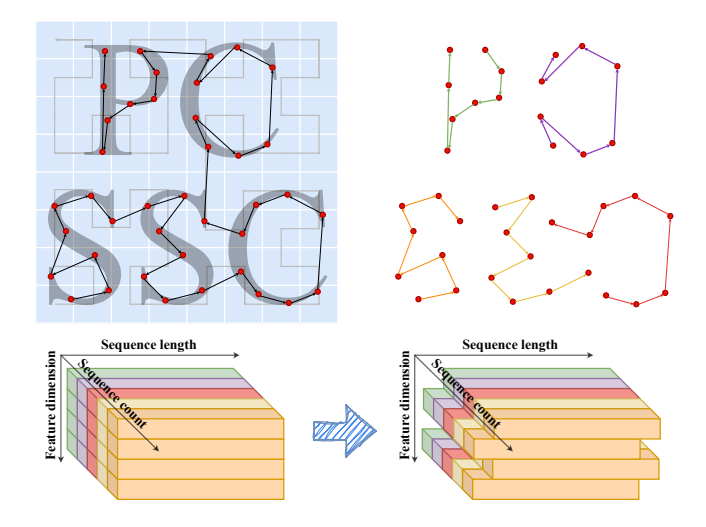


Figure 4: The specific procedure of P-Shift.

In the Channel Mixing module, R_c and K_c are obtained similarly, while V_c is computed as a linear projection of the activated K_c :

$$R_{c} = P-Shift_{R}(X)W_{R},$$

$$K_{c} = P-Shift_{K}(X)W_{K},$$

$$V_{c} = SquaredReLU(K_{c})W_{V}.$$
(9)

The output O_c is obtained by element-wise multiplication of $\sigma(R_c)$ and V_c , followed by a linear projection:

$$O_c = (\sigma(R_c) \odot V_c) W_O. \tag{10}$$

3.6 Training Loss

For the completion task, we use the Chamfer Distance (CD) to evaluate the difference between the predicted point cloud P and the ground truth point cloud \widehat{P} .

$$L_{CD} = \frac{1}{|P|} \sum_{x \in P} \min_{y \in \widehat{P}} ||x - y|| + \frac{1}{|\widehat{P}|} \sum_{y \in \widehat{P}} \min_{x \in P} ||y - x||, \quad (11)$$

where *x* and *y* are points in *P* and \widehat{P} , respectively.

For the semantic segmentation task, we use a weighted negative log-likelihood (NLL) loss to address the challenge of class imbalance. In traditional NLL loss, each class is treated equally, which can lead to suboptimal performance for underrepresented classes. By assigning different weights to each class, we increase the penalty for misclassifying underrepresented classes, thereby encouraging the model to focus more on those classes during training.

The weighted negative log-likelihood loss is defined as:

$$L_{sem} = \sum_{l \in I} -w_l \log(p_l), \tag{12}$$

where l represents the labels associated with the nearest ground-truth points to the predicted points $l \in L$, p_l is the predicted probability, and w is the weight assigned to each class to mitigate class imbalance. In the SSC-PC dataset, w is set to {1.50, 0.96, 1.03, 1.10, 1.67, 1.10, 1.14, 1.74, 0.69, 1.06, 2.09, 1.10, 1.06, 1.57, 1.68, 0.69}.

The overall loss function L_{SSC} combines both Chamfer Distance loss L_{CD} and semantic segmentation loss L_{sem} , balanced by the parameter α :

$$L_{SSC} = \sum_{i=0}^{N} L_{CD}(P_i, \widehat{P}_i) + \alpha L_{sem}(L_i, \widehat{L}_i).$$
 (13)

In Equation (13), α is set to 0.01 for indoor scenes and 0.2 for outdoor scenes due to the larger spatial scale of the latter, P_0 and L_0 represent P_{coarse} and L_{coarse} respectively. When $1 \le i \le N$, P_i and L_i represent the semantic scene point clouds output by RWKV-PD.

4 Experiment

4.1 Dataset Preparation

For point cloud semantic scene completion, existing datasets play a crucial role in evaluating model performance across different settings. Specifically, SSC-PC and NYUCAD-PC primarily address indoor environments, whereas PointSSC serves as a valuable benchmark for outdoor scenes. In addition to these existing datasets, we introduce two new contributions. First, we present NYUCAD-PC-V2, an improved version of NYUCAD-PC that rectifies semantic ambiguities in object labeling, thereby ensuring more reliable annotations. Second, we introduce 3D-FRONT-PC, a novel dataset derived from 3D-FRONT scene models, which offers a broader spectrum of categories and a substantially larger scale.

SSC-PC [17, 58]: This dataset comprises 1941 scenes from 16 object categories in RGB-D format, accompanied by ground-truth point clouds. Due to the absence of camera intrinsics, partial input point clouds are generated using a visibility approximation method. Both input and output point clouds consist of 4096 points, with 1543 scenes designated for training and 398 for testing.

NYUCAD-PC [8, 12, 50]: Comprising 1449 RGB-D images, this dataset includes 795 training and 654 testing samples. The input clouds contain 4096 points, while the ground truth is represented by 8192 points, sampled using Poisson disk sampling. With 11 categories (excluding "empty"), This dataset is more challenging than SSC-PC due to occlusions and incomplete scene coverage.

NYUCAD-PC-V2: Building upon NYUCAD-PC, we introduce NYUCAD-PC-V2, an corrected version of the original dataset. The improvement addresses a significant issue in the original dataset: the semantic confusion caused by adjacent objects being misclassified when they are close to surfaces like walls, floors, or ceilings, which can lead the model to learn incorrect semantic information.

3D-FRONT-PC: The 3D-FRONT-PC dataset is derived from the 3D-FRONT [9] virtual scene dataset provided by Alibaba. It contains 12,655 scene point clouds representing various indoor settings, including 10,124 instances in the training set and 2,531 instances in the test set.

PointSSC: Derived from six intersections in V2X-Seq, PointSSC comprises 11,275 scene point clouds, with each input point cloud containing 26,624 points and the corresponding ground truth comprising 212,992 points. The dataset is divided based on time and scene. The time-based split allocates 80% of the frames for training and 20% for testing, while the scene-based split assigns four intersections for training and the remaining two for testing.

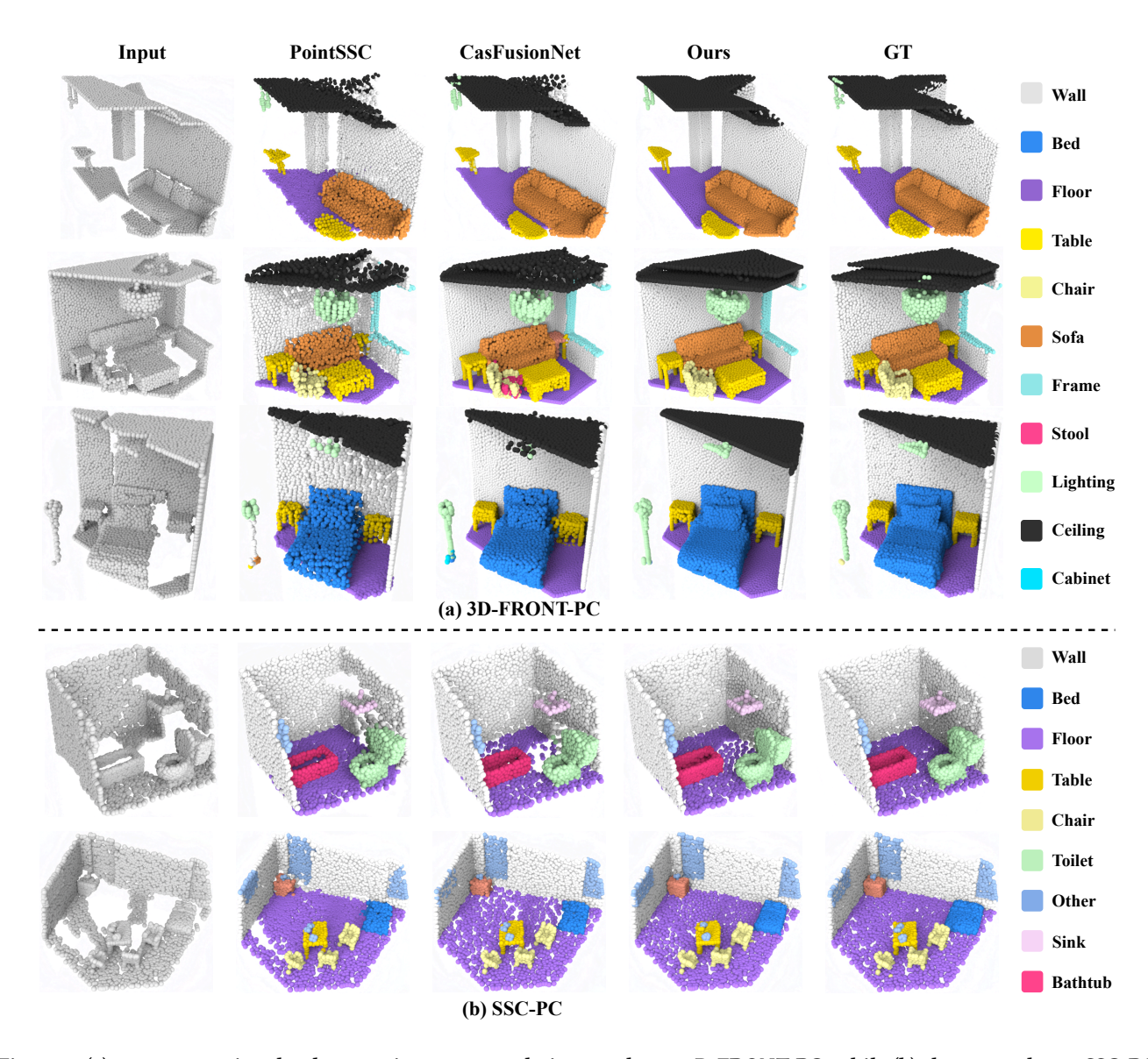


Figure 5: (a) compares point cloud semantic scene completion results on 3D-FRONT-PC, while (b) shows results on SSC-PC.

4.2 Evaluation metrics and Implementation

Evaluation metrics. For evaluating scene completion performance, we employ Chamfer Distance (CD) and F1-score. For semantic segmentation, we assess performance using the mean class Intersection over Union (mIoU) and the mean class accuracy (mAcc).

Implementation. We implement our network in PyTorch and train it on a single Nvidia RTX 3090 GPU for 100 epochs with a batch size of 8. The AdamMax optimizer is used with an initial learning rate of 0.0075, which decayes by a factor of 0.99 every 2 epochs. The balance parameter α in Eq. 13 is set to 0.01. Furthermore, taking into account both performance and model complexity, we employ a three-stage RWKV-PD for indoor scenes and a single-stage RWKV-PD for outdoor scenes.

4.3 Quantitative and Qualitative Results

We compared our proposed method with recent point-based semantic scene completion networks, including PCSSC-Net [58], Cas-FusionNet [50], and PointSSC [51], to evaluate its effectiveness and robustness. To ensure a fair and rigorous comparison, we retrained the publicly available CasFusionNet code on our newly prepared NYUCAD-PC-V2 and 3D-FRONT-PC datasets. Additionally, we trained PointSSC using its publicly accessible code on all indoor scenes. Notably, for PointSSC-scene-split, PointSSC integrates both point clouds and images as inputs, whereas our method relies solely on point clouds. The remaining data were obtained from the published evaluation metrics of PCSSC-Net, CasFusionNet, and PointSSC to ensure objective comparison.

Table 1: Quantitative comparison of methods on different indoor datasets. CD refers to Chamfer Distance L2 (multiplied by 10³),F1-score means calculating by distance threshold 0.01. mIoU is the mean Intersection over Union, and mAcc represents mean Accuracy. The best results are in Bold.

Method	SSC-PC					NYUCA	AD-PC			NYUCAI	D-PC-V2		3D-FRONT-PC						
	CD↓	F1-Score ↑	mAcc ↑	mIoU ↑	CD↓	F1-Score ↑	mAcc ↑	mIoU ↑	CD↓	F1-Score ↑	mAcc ↑	mIoU ↑	CD↓	F1-Score ↑	mAcc ↑	mIoU ↑			
PCSSC-Net[58]	1.58	-	-	88.2	-	-	-	-	-	-	-	-	-	-	-	-			
CasFusionNet[50]	0.426	54.00%	95.11	91.94	1.164	75.19%	59.75	49.46	1.369	74.18%	60.77	50.42	0.218	84.95%	61.31	52.69			
PointSSC[51]	0.614	51.02%	88.32	82.52	2.745	65.99%	52.05	42.12	2.698	64.96%	54.84	44.70	0.251	79.37%	61.06	55.33			
Ours	0.265	66.93%	97.99	95.27	1.116	76.30%	66.47	54.52	1.104	76.77%	68.49	56.79	0.171	89.21%	78.33	64.27			

Table 2: Quantitative comparison of methods on outdoor dataset PointSSC-time-split and PointSSC-scene-split[51]. CD refers to Chamfer Distance L1 (multiplied by 10³),F1-score means calculating by distance threshold 0.3. The best results are in Bold.

Method	Poi	ntSSC-time-s	plit	PointSSC-scene-split								
memou	CD↓	F1-Score ↑	mIoU ↑	CD↓	F1-Score ↑	mIoU ↑						
CasFusionNet[50]	467.76	70.84%	45.76	664.85	43.98%	11.52						
PointSSC[51]	208.94	81.42%	50.58	410.92	63.57%	14.64						
Ours	179.03	87.72%	60.30	361.58	64.18%	17.23						

Quantitative Results. As shown in Table 1, we evaluated our method on four indoor datasets: SSC-PC, NYUCAD-PC, NYUCAD-PC-V2 and 3D-FRONT-PC, as well as outdoor datasets: PointSSC-time-split and PointSSC-scene-split, comparing its performance against the indoor baseline CasFusionNet and the outdoor baseline PointSSC. On the SSC-PC dataset, our method reduces the mAcc inaccuracy rate from 4.89% to 2.01%, achieving an approximate 58.9% reduction. Furthermore, the CD L2 metric (multiplied by 10³) is reduced from 0.426 to 0.265. In the outdoor scenario of PointSSC-time-split, our method significantly enhances performance, increasing the mIoU from 50.58% to 60.30%. Meanwhile, the CD L1 metric (multiplied by 10³) is reduced from 208.94 to 179.03.

Qualitative results. Figure 5 further presents qualitative comparisons on two datasets. Figure 5 (a) shows three scenes from the 3D-FRONT-PC dataset, while Figure 5 (b) displays two scenes from the SSC-PC [58] dataset. From the visual comparisons, our method exhibits superior performance in both segmentation and completion tasks, effectively preserving and reconstructing fine details.

4.4 Ablation Study

To evaluate the effectiveness of the major components in our method, we conducted an ablation study on the SSC-PC dataset by simplifying our network under the following configurations:

Model A: We remove the RWKV-SG module, and adopt CasFusionNet [50] approach that utilizes global features to predict semantic labels with MLPs and applies FPS to obtain a coarse point cloud.

Model B: We combine the Snowflake Point Deconvolution (SPD) module[49] with our Segment Head and Rebuild Head to replace the RWKV-PD module.

Table 3: Comparison of different models for scene completion and semantic segmentation.

Model	Scene completion	Semantic	segmentation
1110 401	CD (×10 ⁻³)	mAcc	mIoU
A	0.353	97.49	94.13
В	0.274	97.26	94.61
C	0.287	97.72	94.48
Ours	0.265	97.99	95.27

Model C: We set the number of layers in the RWKV-PD module to 1 layer, reducing the complexity of the model and evaluating the performance with fewer layers.

Subsequent to the ablation study, we observe that each modification to the model leads to distinct changes in performance.

Specifically, Model A, which replaces the RWKV-SG module with MLPs and FPS, results in a notable increase in Chamfer Distance. This demonstrates that the coarse point cloud and pointwise features generated by RWKV-SG significantly contribute to the subsequent coarse-to-fine process. Model B, after replacing the RWKV-PD module, failed to effectively capture finer spatial and sementic details, leading to lower performance in both scene completion and segmentation accuracy. Model C, which simplifies the RWKV-PD module by reducing its number of layers to just one, leads to a performance drop across both scene completion and semantic segmentation tasks. This indicates that the additional layers in the RWKV-PD module are essential for capturing the complexity of point-wise features.

5 Conclusion

In this work, we introduce RWKV-PCSSC, a lightweight point cloud semantic scene completion network inspired by the RWKV mechanism. The network comprises two key components: the RWKV Seed Generator (RWKV-SG), which aggregates features from partial point clouds to generate a coarse representation, and the RWKV Point Deconvolution (RWKV-PD) modules, which progressively restore point-wise features. Our method achieves state-of-the-art performance on both indoor and outdoor datasets, while significantly reducing the number of parameters and memory usage.

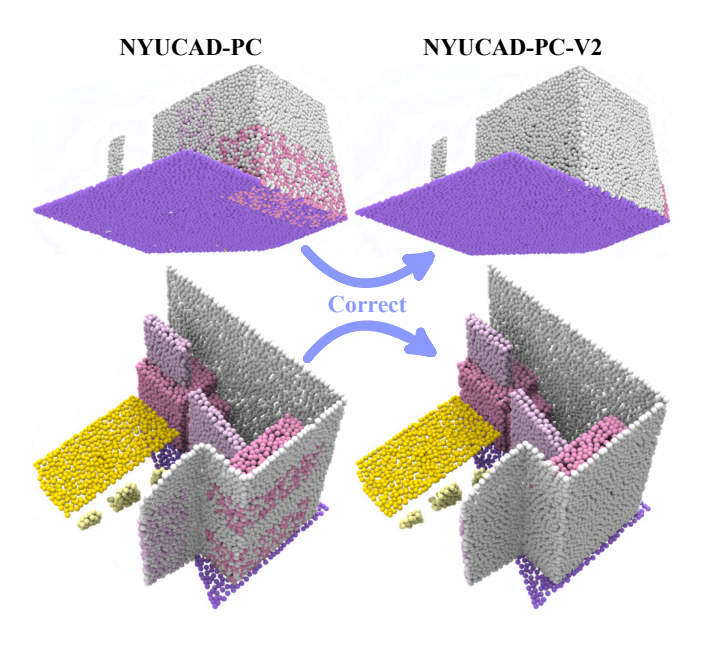


Figure 6: The issue of label confusion in the point clouds within the NYUCAD-PC dataset, along with the corrections made in the NYUCAD-PC-V2 dataset.

6 Dataset Details

NYUCAD-PC-V2: We present NYUCAD-PC-V2, an enhanced version of the NYUCAD-PC dataset that addresses semantic misclassifications of adjacent objects near surfaces such as walls, floors, and ceilings, as shown in Figure 6. To resolve this, we reassign points located within 0.005 distance of walls, floors, and ceilings to the corresponding mesh label of the nearest surface. This refinement leads to a more accurate semantic segmentation, where surfaces are better distinguished from attached objects.

3D-FRONT-PC Dataset: The 3D-FRONT-PC dataset is derived from the Alibaba-provided 3D-FRONT virtual scene dataset [9], comprising 12,655 indoor scene point clouds with diverse settings. It consists of 10,124 training instances and 2,531 test instances.

To generate the input point cloud P_{in} , we employ raycasting to render three-dimensional scenes into two-dimensional depth images via a pinhole camera model. Specifically, we define the intrinsic parameters (focal length and optical center) and extrinsic parameters (position, orientation, and field of view) of the camera, and set the output image resolution. Based on these parameters, rays are generated from the camera's viewpoint, traversing each pixel of the image plane and simulating intersections with the scene. These rays are cast into the three-dimensional scene, and the distances of their first intersections with the scene surfaces are recorded and organized into a depth image, where each pixel value represents the Euclidean distance from the camera to the scene surface. The depth information is then converted into a point cloud by integrating the depth image with the camera's intrinsic parameters and back-projecting each pixel based on its depth value, resulting in $P_i n$ that encapsulates geometric information.

To acquire the ground truth points P_{gt} within the camera's field of view (FoV), we first generate a dense scene point cloud P_{scene}

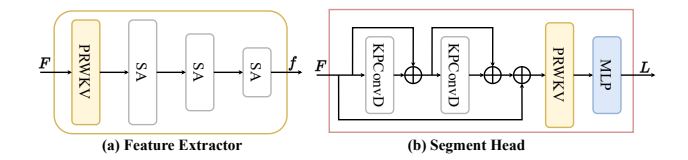


Figure 7: (a) The detailed architecture of the Feature Extractor. (b) The detailed architecture of the Segment Head.

through Poisson sampling on the 3D mesh representation of the environment. The sampling density is configured to ensure uniform coverage of surface geometries. We subsequently perform frustum culling on P_{scene} using a near clipping plane at 0.2 m, far clipping plane at 6 m, and 60° FoV. Points satisfying both the depth constraint and the angular bounds are retained as candidates for visible ground truth. Finally, Farthest Point Sampling (FPS) is applied to P_{scene} and the visible subset to obtain downsampled point clouds of 4096 and 8192 points respectively.

7 Additional Notes on Modules

The detailed architectures of the Feature Extractor and the Segment Head are depicted in Figure 6 (a) and Figure 6 (b), respectively. The Feature Extractor utilizes a PRWKV module to capture and integrate global contextual information, followed by a series of Set Abstraction layers to progressively refine local point features, culminating in a comprehensive global feature representation, denoted as f. On the other hand, the Segment Head employs KPConvD[37] with residual connections to extract local features from the point cloud, thereby improving feature stability and alleviating gradient vanishing. It then leverages the PRWKV module to abstract global information, effectively modeling long-range dependencies and contextual relationships within the point cloud. Finally, the processed features are fed into an MLP to generate the semantic prediction outputs L.

8 Additional Charts and Results

Due to page limitations, we present only the overall performances in the main text. For comprehensive results, detailed metrics for different models across the PointSSC, SSC-PC, NYUCAD-PC, NYUCAD-PC-V2, and 3D-FRONT-PC datasets are provided in the supplementary material, as demonstrated in Table 4, Table 5, Table 6, Table 7, and Table 8. Figure 8 provides the qualitative comparisons on PointSSC, and Figure 9 illustrates the qualitative comparisons on NYUCAD-PC-V2.

Table 4: Quantitative comparison of different methods on PointSSC dataset. CD Means Chamfer Distance(Multiplied By 1000), lower is better. F1-score@0.3 means calculating by distance threshold 0.3. The best results are in Bold. Additionally, PointSSC utilizes both point clouds and images as inputs for Scene Splitting, whereas our method relies solely on point clouds.

_	Methods	$CD(L_1)\downarrow$	$CD(L_2)\downarrow$	F1-Score@0.3↑	mIoU ↑	building	tree	road	sidewalk	person	plant	car	fence	signboard	bus	truck	streetlight	barricade	van	bicycle	motorcyclist
	FoldingNet[52]	610.30	2785.44	39.65%	14.91	8.56	60.74	81.01	27.45	0.00	35.26	12.31	11.24	1.07	0.14	0.70	0.00	0.00	0.00	0.00	0.00
	PCN[56]	317.38	510.19	64.46%	12.65	0.14	69.71	83.91	0.70	0.00	29.76	2.08	9.05	7.05	0.01	0.00	0.00	0.01	0.00	0.00	0.00
50	PoinTr[54]	3864.43	129947.08	15.66%	5.21	0.00	2.69	0.00	0.00	0.00	0.00	2.52	0.00	0.00	0.00	0.00	0.00	0.00	0.00	0.00	0.00
£	SnowFlakeNet[49]	461.89	2846.09	52.99%	20.78	11.58	80.65	80.79	32.47	0.00	48.84	1.47	35.63	36.34	2.03	1.47	1.14	0.00	0.00	0.00	0.00
Splitting	PMP-Net++[45]	541.82	3753.60	57.09%	25.25	21.79	80.67	87.89	10.10	4.73	37.53	44.29	14.53	7.74	37.97	29.66	3.20	19.02	3.83	0.00	1.04
e S	CasFusionNet[50]	467.76	5087.18	70.84%	45.76	55.20	90.50	90.11	55.08	19.52	69.91	59.38	58.46	45.35	47.89	37.62	12.53	9.66	39.85	13.80	27.37
ä	AdaPoinTr[55]	237.11	290.71	78.79%	45.09	45.53	87.08	93.42	53.36	13.00	64.46	55.99	56.41	42.36	56.44	37.56	15.79	17.61	43.05	11.31	28.07
	PointSSC[51]	208.94	248.28	81.42%	50.58	61.42	90.94	92.41	63.32	13.40	74.33	66.17	67.53	47.93	61.37	44.35	14.92	18.82	43.69	17.64	31.07
	RWKV-PCSSC (Ours)	179.026	166.346	87.72%	60.30	66.45	92.48	91.46	65.66	38.04	76.59	67.6	68.4	53.6	68.56	58.69	30.95	29.17	56.86	40.29	60.05
	FoldingNet[52]	1146.07	16950.85	6.06%	8.11	0.14	8.79	84.06	4.08	0.00	31.60	1.01	0.00	0.00	0.00	0.00	0.00	0.00	0.00	0.00	0.00
	PCN[56]	809.55	5778.96	42.66%	8.62	0.03	47.95	78.07	0.01	0.00	11.86	0.00	0.00	0.02	0.00	0.00	0.00	0.00	0.00	0.00	0.00
50	PoinTr[54]	4164.05	90275.69	15.89%	0.40	0.00	0.00	0.02	0.01	0.00	0.00	6.06	0.00	0.00	0.00	0.24	0.00	0.00	0.00	0.00	0.00
#	SnowFlakeNet[49]	1055.09	21849.79	42.36%	8.09	0.00	55.81	63.33	2.06	0.00	7.51	0.00	0.00	0.26	0.18	0.00	0.35	0.00	0.00	0.00	0.00
Split	PMP-Net++[45]	530.80	3753.60	57.09%	13.66	0.00	65.75	84.76	8.80	0.00	16.32	24.66	0.01	0.86	4.96	5.17	0.00	0.71	4.94	0.00	1.57
9	CasFusionNet[50]	664.85	8310.55	43.98%	11.52	0.52	62.33	65.68	6.04	0.08	9.06	21.84	0.00	0.48	8.08	0.12	0.18	0.00	7.06	0.92	1.85
cer	AdaPoinTr[55]	493.41	3098.48	61.41%	13.20	0.43	66.38	84.91	5.57	0.00	15.86	15.67	0.00	0.21	1.90	5.07	1.55	0.00	11.55	0.06	2.06
S	PointSSC[51]	410.92	1413.60	63.57%	14.64	0.12	68.93	85.68	14.02	0.00	13.22	24.69	10.64	1.78	1.32	5.65	0.01	0.07	5.42	0.54	2.13
	RWKV-PCSSC (Ours)	361.58	1560.67	64.18%	17.23	1.20	60.24	79.79	10.18	2.25	20.61	38.13	0.09	11.24	8.89	1.03	0.10	0.00	23.58	6.89	14.53

Table 5: Quantitative comparison of different methods on SSC-PC dataset. CD Means Chamfer Distance(Multiplied By 1000), lower is better. F1-score@0.01 means calculating by distance threshold 0.01. The best results are in Bold. In the original PCSSC-Net paper [23], IoU was reported for only 13 categories in the SSC-PC dataset, while the remaining three categories were denoted as "-".

Methods	CD $(L_1) \downarrow$	$\mathrm{CD}\left(L_{2}\right)\downarrow$	F1-Score@0.01 ↑	mIoU ↑	Bathtub	bed	bookshelf	cabinet	ceiling	chair	desk	door	floor	other	sink	sofa	table	toilet	tv	wall
PCSSC-Net[23]	-	1.58	-	88.2	90.5	96.9	84.9	79.0	-	83.7	87.4	89.1	99.1	-	89.2	87.7	86.0	86.5	-	97.5
CasFusionNet[50]	9.413	0.425	54.00%	91.94	90.55	96.81	94.55	89.92	96.43	92.80	87.44	87.64	93.17	73.38	99.62	91.32	91.71	93.70	95.57	96.50
PointSSC[51]	11.543	0.614	51.02%	82.52	73.06	90.22	78.62	80.05	92.29	79.88	77.04	73.45	91.02	57.29	99.29	80.47	85.11	79.95	93.33	89.30
RWKV-PCSSC (Ours)	6.937	0.265	66.93%	95.27	95.77	97.66	96.70	95.63	97.28	95.72	95.33	93.87	93.46	81.68	99.38	95.30	95.21	96.35	98.03	96.93

Table 6: Quantitative comparison of different methods on NYUCAD-PC dataset. CD Means Chamfer Distance(Multiplied By 1000), lower is better. F1-score@0.01 means calculating by distance threshold 0.01. The best results are in Bold.

Methods	$\mid \operatorname{CD}(L_1) \downarrow$	$CD(L_2)\downarrow$	F1-Score@0.01 ↑	mIoU↑	ceiling	floor	wall	window	chair	bed	sofa	table	tvs	furnsink	objs
CasFusionNet[50]	10.276	1.164	75.19%	49.46	76.48	87.35	67.33	8.40	62.74	52.73	47.26	48.90	14.30	44.04	34.57
PointSSC[51]	13.898	2.745	65.99%	42.12	80.40	84.32	60.58	6.83	43.67	44.28	37.39	35.26	8.69	37.59	24.24
RWKV-PCSSC (Ours)	10.128	1.116	76.30%	54.52	81.22	87.71	70.60	20.29	66.83	61.78	57.94	53.13	15.92	46.89	37.37

Table 7: Quantitative comparison of different methods on NYUCAD-PC-V2 dataset. CD Means Chamfer Distance(Multiplied By 1000), lower is better. F1-score@0.01 means calculating by distance threshold 0.01. The best results are in Bold.

Methods	$\mid \operatorname{CD}(L_1) \downarrow$	$CD(L_2)\downarrow$	F1-Score@0.01 ↑	mIoU↑	ceiling	floor	wall	window	chair	bed	sofa	table	tvs	furnsink	objs
CasFusionNet[50] PointSSC[51]	10.410 14.131	1.369 2.698	74.18 64.9550	50.42 44.70	80.35 77.70	96.29 95.84	71.29 67.72	10.45 4.35	63.80 38.85	56.21 55.98	42.01 37.42	48.02 36.83	10.63 10.56	44.44 42.46	31.17 24.03
RWKV-PCSSC (Ours)	10.126	1.104	76.767	56.79	80.94	96.27	76.96	18.36	69.41	67.64	58.08	55.31	10.60	51.42	39.71

Table 8: Quantitative comparison of different methods on 3D-FRONT-PC dataset. CD Means Chamfer Distance(Multiplied By 1000), lower is better. F1-score@0.01 means calculating by distance threshold 0.01. The best results are in Bold.

Methods	$CD(L_1)\downarrow$	$CD(L_2)\downarrow$	F1-Score@0.01↑	mIoU ↑	cabinet	pier	bed	chair	table	sofa	lighting	storage	electric	decor	sink	attachment	plants	wall	ceiling	floor	openings	pipe	stair	others
CasFusionNet[50]	6.947	0.218	84.95	52.69	46.19	22.01	76.18	75.48	74.32	79.38	85.83	44.07	39.43	21.83	45.45	22.46	45.99	84.20	90.31	92.85	69.97	36.14	1.50	40.81
PointSSC[51]	7.627	0.251	79.368	55.33	41.60	24.49	80.22	79.55	81.02	83.29	90.70	37.57	30.06	18.64	37.22	1.66	48.96	87.88	86.95	91.37	71.44	31.02	0.00	30.06
RWKV-PCSSC (Ours)	6.421	0.171	89.21	64.27	55.57	53.95	88.63	86.54	86.88	89.35	92.15	54.33	46.21	39.15	64.66	50.42	66.06	88.74	90.83	91.12	77.59	7.81	4.85	50.52

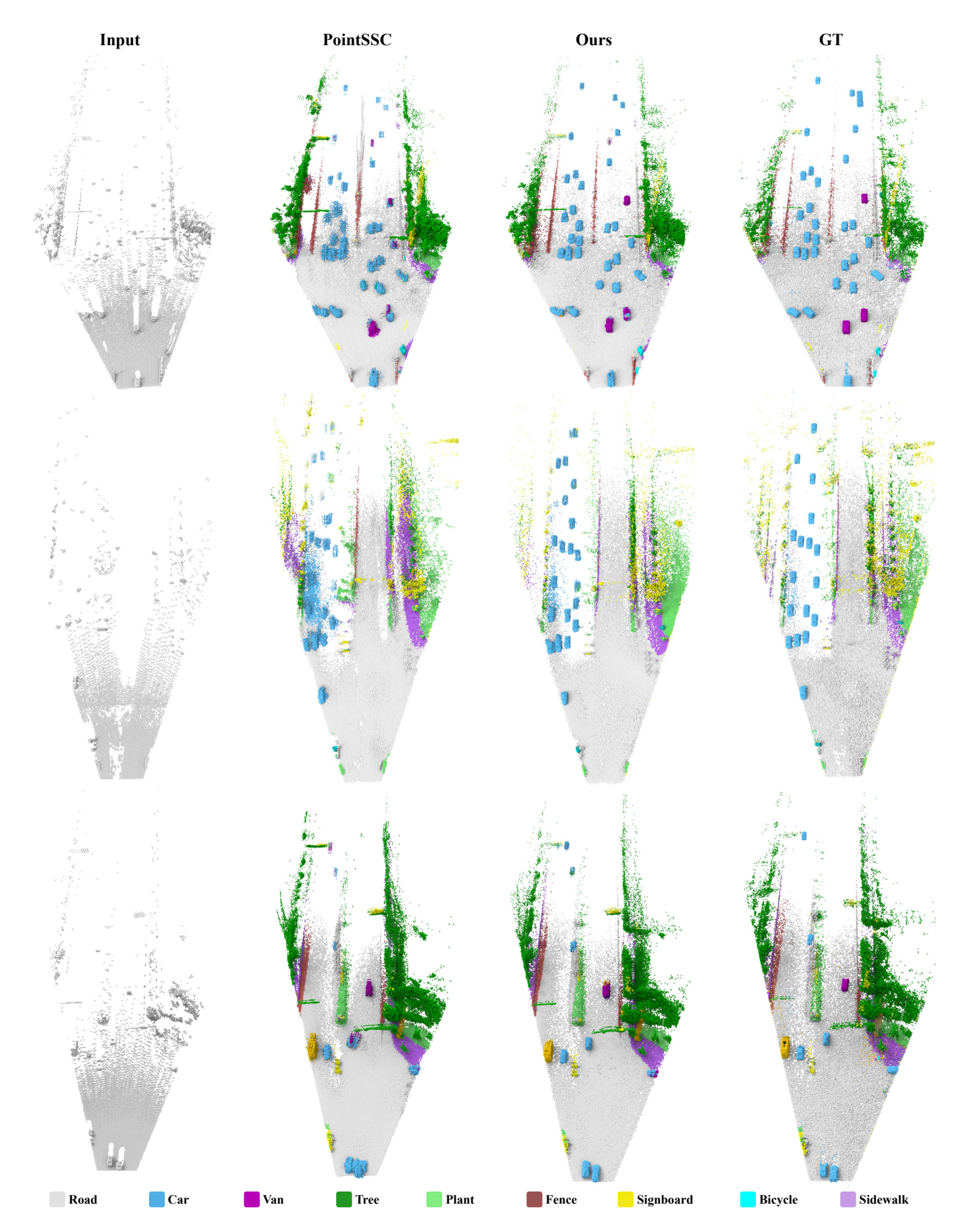


Figure 8: Visualization results on the PointSSC dataset

Acknowledgments

The work is supported by National Key Research and Development Program of China (2025YFB3003600), National Natural Science Foundation of China (No.62202151) and (No.62202152).

References

- Xiaokang Chen, Kwan-Yee Lin, Chen Qian, Gang Zeng, and Hongsheng Li. 2020.
 3D Sketch-aware Semantic Scene Completion via Semi-supervised Structure Prior. In CVPR. 4193–4202.
- [2] Xu Chenfeng, Wu Bichen, Wang Zining, Zhan Wei, Vajda Peter, Keutzer Kurt, and Tomizuka Masayoshi. 2020. SqueezeSegV3: Spatially-Adaptive Convolution for Efficient Point-Cloud Segmentation. In European Conference on Computer Vision. 1–19.
- [3] Aloisio Dourado, Teofilo E De Campos, Hansung Kim, and Adrian Hilton. 2021.
 EdgeNet: Semantic Scene Completion from a Single RGB-D Image. In ICPR. IEEE, 503-510
- [4] Aloisio Dourado, Frederico Guth, and Teofilo de Campos. 2022. Data Augmented 3D Semantic Scene Completion with 2D Segmentation Priors. In Proceedings of the IEEE/CVF Winter Conference on Applications of Computer Vision. 3781–3790.
- [5] Yuchen Duan, Weiyun Wang, Zhe Chen, Xizhou Zhu, Lewei Lu, Tong Lu, Yu Qiao, Hongsheng Li, Jifeng Dai, and Wenhai Wang. 2024. Vision-RWKV: Efficient and Scalable Visual Perception with RWKV-Like Architectures. arXiv preprint arXiv:2403.02308 (2024).
- [6] Yuchen Duan, Weiyun Wang, Zhe Chen, Xizhou Zhu, Lewei Lu, Tong Lu, Yu Qiao, Hongsheng Li, Jifeng Dai, and Wenhai Wang. 2025. Vision-RWKV: Efficient and Scalable Visual Perception with RWKV-Like Architectures. ICLR (2025).
- [7] Zhengcong Fei, Mingyuan Fan, Changqian Yu, Debang Li, and Junshi Huang. 2024. Diffusion-RWKV: Scaling RWKV-Like Architectures for Diffusion Models. CoRR abs/2404.04478 (2024).
- [8] Michael Firman, Oisin Mac Aodha, Simon Julier, and Gabriel J Brostow. 2016. Structured Prediction of Unobserved Voxels From a Single Depth Image. In CVPR. 5431–5440.
- [9] Huan Fu, Bowen Cai, Lin Gao, Ling-Xiao Zhang, Jiaming Wang, Cao Li, Qixun Zeng, Chengyue Sun, Rongfei Jia, Binqiang Zhao, et al. 2021. 3d-front: 3d furnished rooms with layouts and semantics. In Proceedings of the IEEE/CVF International Conference on Computer Vision. 10933–10942.
- [10] Huan Fu, Rongfei Jia, Lin Gao, Mingming Gong, Binqiang Zhao, Steve Maybank, and Dacheng Tao. 2021. 3d-future: 3d furniture shape with texture. *International Journal of Computer Vision* (2021), 1–25.
- [11] Meng-Hao Guo, Jun-Xiong Cai, Zheng-Ning Liu, Tai-Jiang Mu, Ralph R. Martin, and Shi-Min Hu. 2021. PCT: Point Cloud Transformer. Computational Visual Media 7, 2 (2021), 187–199.
- [12] Ruiqi Guo, Chuhang Zou, and Derek Hoiem. 2015. Predicting Complete 3D Models of Indoor Scenes. arXiv preprint arXiv:1504.02437 (2015).
- [13] Saurabh Gupta, James Davidson, Sergey Levine, Rahul Sukthankar, and Jitendra Malik. 2017. Cognitive Mapping and Planning for Visual Navigation. In CVPR. 2616–2625.
- [14] Xu Han, Yuan Tang, Zhaoxuan Wang, and Xianzhi Li. 2024. Mamba3D: Enhancing Local Features for 3D Point Cloud Analysis Via State Space Model. Proceedings of the 32nd ACM International Conference on Multimedia (2024), 4995–5004.
- [15] Qingdong He, Jiangning Zhang, Jinlong Peng, Haoyang He, Yabiao Wang, and Chengjie Wang. 2025. PointRWKV: Efficient RWKV-Like Model for Hierarchical Point Cloud Learning. AAAI (2025).
- [16] David Hilbert and David Hilbert. 1935. Über die stetige Abbildung einer Linie auf ein Flächenstück. Dritter Band: Analysis Grundlagen der Mathematik Physik Verschiedenes: Nebst Einer Lebensgeschichte (1935), 1–2.
- [17] Sagi Katz, Ayellet Tal, and Ronen Basri. 2007. Direct Visibility of Point Sets. In ACM Transactions on Graphics (SIGGRAPH). 24–es.
- [18] Xin Lai, Jianhui Liu, Li Jiang, Liwei Wang, Hengshuang Zhao, Shu Liu, Xiaojuan Qi, and Jiaya Jia. 2022. Stratified Transformer for 3D Point Cloud Segmentation. Proceedings - IEEE Computer Society Conference on Computer Vision and Pattern Recognition abs/2203.14508 (2022).
- [19] Haoang Li, Jinhu Dong, Binghui Wen, Ming Gao, Tianyu Huang, Yun-Hui Liu, and Daniel Cremers. 2023. DDIT: Semantic Scene Completion Via Deformable Deep Implicit Templates.. In IEEE International Conference on Computer Vision. 21804—21904
- [20] Jie Li, Kai Han, Peng Wang, Yu Liu, and Xia Yuan. 2020. Anisotropic Convolutional Networks for 3D Semantic Scene Completion. In CVPR. 3351–3359.
- [21] Jie Li, Peng Wang, Kai Han, and Yu Liu. 2021. Anisotropic Convolutional Neural Networks for RGB-D Based Semantic Scene Completion. IEEE Transactions on Pattern Analysis and Machine Intelligence (2021), 1–1.
- [22] Dingkang Liang, Xin Zhou, Wei Xu, Xingkui Zhu, Zhikang Zou, Xiaoqing Ye, Xiao Tan, and Xiang Bai. 2024. PointMamba: A Simple State Space Model for Point Cloud Analysis. In Advances in Neural Information Processing Systems.

- [23] Yiqing Liang, Boyuan Chen, and Shuran Song. 2021. SSCNav: Confidence-Aware Semantic Scene Completion for Visual Semantic Navigation. In 2021 IEEE International Conference on Robotics and Automation (ICRA). IEEE, 13194–13200.
- [24] Minghua Liu, Lu Sheng, Sheng Yang, Jing Shao, and Shi-Min Hu. 2020. Morphing and Sampling Network for Dense Point Cloud Completion. In AAAI, Vol. 34. 11596–11603.
- [25] Xianzhu Liu, Haozhe Xie, Shengping Zhang, Hongxun Yao, Rongrong Ji, Liqiang Nie, and Dacheng Tao. 2024. 2D Semantic-Guided Semantic Scene Completion. International Journal of Computer Vision (2024), 1–20.
- [26] Xu Ma, Can Qin, Haoxuan You, Haoxi Ran, and Yun Fu. 2022. Rethinking Network Design and Local Geometry in Point Cloud: A Simple Residual MLP Framework. Computing Research Repository abs/2202.07123 (2022).
- [27] Guy M. Morton. 1966. A computer oriented geodetic data base and a new technique in file sequencing. physics of plasmas (1966).
- [28] Bo Peng, Eric Alcaide, Quentin Anthony, Alon Albalak, Samuel Arcadinho, Huanqi Cao, Xin Cheng, Michael Chung, Matteo Grella, Kranthi Kiran GV, et al. 2023. RWKV: Reinventing RNNs for the Transformer Era. arXiv preprint arXiv:2305.13048 (2023).
- [29] Charles R. Qi, Hao Su, Kaichun Mo, and Leonidas J. Guibas. 2016. PointNet: Deep Learning on Point Sets for 3D Classification and Segmentation. Proceedings -IEEE Computer Society Conference on Computer Vision and Pattern Recognition abs/1612.00593 (2016), 77–85.
- [30] Charles Ruizhongtai Qi, Li Yi, Hao Su, and Leonidas J Guibas. 2017. PointNet++: Deep Hierarchical Feature Learning on Point Sets in a Metric Space. In Advances in Neural Information Processing Systems, Vol. 30.
- [31] Guocheng Qian, Yuchen Li, Houwen Peng, Jinjie Mai, Hasan Abed Al Kader Hammoud, Mohamed Elhoseiny, and Bernard Ghanem. 2022. PointNeXt: Revisiting PointNet++ with Improved Training and Scaling Strategies.. In Conference on Neural Information Processing Systems.
- [32] Yi Rong, Haoran Zhou, Lixin Yuan, Cheng Mei, Jiahao Wang, and Tong Lu. 2024. CRA-PCN: Point Cloud Completion with Intra- and Inter-level Cross-Resolution Transformers. Proceedings of the AAAI Conference on Artificial Intelligence 38, 5 (2024), 4676–4685.
- [33] Shuran Song, Fisher Yu, Andy Zeng, Angel X Chang, Manolis Savva, and Thomas Funkhouser. 2017. Semantic Scene Completion from a Single Depth Image. In CVPR. 1746–1754.
- [34] Lyne P. Tchapmi, Vineet Kosaraju, Hamid Rezatofighi, Ian D. Reid, and Silvio Savarese. 2019. TopNet: Structural Point Cloud Decoder. Proceedings - IEEE Computer Society Conference on Computer Vision and Pattern Recognition (2019), 383–392.
- [35] Gusi Te, Wei Hu, Zongming Guo, and Amin Zheng. 2018. RGCNN: Regularized Graph CNN for Point Cloud Segmentation.. In ACM International Conference on Multimedia. 746–754.
- [36] Hugues Thomas, Charles R. Qi, Jean-Emmanuel Deschaud, Beatriz Marcotegui, François Goulette, and Leonidas J. Guibas. 2019. KPConv: Flexible and Deformable Convolution for Point Clouds. Proceedings of the IEEE International Conference on Computer Vision (2019).
- [37] Hugues Thomas, Yao-Hung Hubert Tsai, Timothy Barfoot, and Jian Zhang. 2024. KPConvX: Modernizing Kernel Point Convolution with Kernel Attention. CVPR 2024 (2024).
- [38] Jacob Varley, Chad DeChant, Adam Richardson, Joaquín Ruales, and Peter Allen. 2017. Shape Completion Enabled Robotic Grasping. In 2017 IEEE/RSJ International Conference on Intelligent Robots and Systems (IROS). IEEE, 2442–2447.
- [39] Fengyun Wang, Dong Zhang, Hanwang Zhang, Jinhui Tang, and Qianru Sun. 2023. Semantic Scene Completion with Cleaner Self. Computer Vision and Pattern Recognition (2023), 867–877.
- [40] Jun Wang, Ying Cui, Dongyan Guo, Junxia Li, Qingshan Liu, and Chunhua Shen. 2024. PointAttN: You Only Need Attention for Point Cloud Completion. Proceedings of the AAAI Conference on Artificial Intelligence 38, 6 (2024), 5472– 5480.
- [41] Junming Wang, Wei Yin, Xiaoxiao Long, Xinyu Zhang, Zebing Xing, Xiaoyang Guo, and Zhang Qian. 2025. OccRWKV: Rethinking Efficient 3D Semantic Occupancy Prediction with Linear Complexity. In 2025 IEEE International Conference on Robotics and Automation (ICRA).
- [42] Xuzhi Wang, Wei Feng, and Liang Wan. 2024. Multi-modal Fusion Architecture Search for Camera-Based Semantic Scene Completion. Expert Systems with Applications 243 (2024).
- [43] Yue Wang, Yongbin Sun, Ziwei Liu, Sanjay E. Sarma, Michael M. Bronstein, and Justin M. Solomon. 2018. Dynamic Graph CNN for Learning on Point Clouds. ACM Transactions on Graphics (2018).
- [44] Xin Wen, Peng Xiang, Zhizhong Han, Yan-Pei Cao, Pengfei Wan, Wen Zheng, and Yu-Shen Liu. 2021. PMP-Net: Point Cloud Completion by Learning Multi-step Point Moving Paths. In CVPR. 7443–7452.
- [45] Xin Wen, Peng Xiang, Zhizhong Han, Yan-Pei Cao, Pengfei Wan, Wen Zheng, and Yu-Shen Liu. 2022. PMP-Net++: Point Cloud Completion by Transformer-Enhanced Multi-step Point Moving Paths. IEEE TPAMI (2022).
- [46] Wenxuan Wu, Zhongang Qi, and Li Fuxin. 2018. PointConv: Deep Convolutional Networks on 3D Point Clouds. Computer Vision and Pattern Recognition

- abs/1811.07246 (2018), 9613-9622.
- [47] Xiaoyang Wu, Li Jiang, Peng-Shuai Wang, Zhijian Liu, Xihui Liu, Yu Qiao, Wanli Ouyang, Tong He, and Hengshuang Zhao. 2024. Point Transformer V3: Simpler, Faster, Stronger. In CVPR.
- [48] Xiaoyang Wu, Yixing Lao, Li Jiang, Xihui Liu, and Hengshuang Zhao. 2022. Point Transformer V2: Grouped Vector Attention and Partition-based Pooling. NeurIPS 2022 (2022).
- [49] Peng Xiang, Xin Wen, Yu-Shen Liu, Yan-Pei Cao, Pengfei Wan, Wen Zheng, and Zhizhong Han. 2021. Snowflake Point Deconvolution for Point Cloud Completion and Generation with Skip-Transformer. In ICCV. 5499–5509.
- [50] Jinfeng Xu, Xianzhi Li, Yuan Tang, Qiao Yu, Yixue Hao, Long Hu, and Min Chen. 2023. CasFusionNet: A Cascaded Network for Point Cloud Semantic Scene Completion by Dense Feature Fusion. THIRTY-SEVENTH AAAI CONFERENCE ON ARTIFICIAL INTELLIGENCE, VOL 37 NO 3 (2023).
- [51] Yuxiang Yan, Boda Liu, Jianfei Ai, Qinbu Li, Ru Wan, and Jian Pu. 2024. PointSSC: A Cooperative Vehicle-Infrastructure Point Cloud Benchmark for Semantic Scene Completion. In 2024 IEEE International Conference on Robotics and Automation (ICRA). IEEE, 17027–17034.
- [52] Yaoqing Yang, Chen Feng, Yiru Shen, and Dong Tian. 2018. Foldingnet: Point cloud auto-encoder via deep grid deformation. In Proceedings of the IEEE conference on computer vision and pattern recognition. 206–215.
- [53] Zhiwen Yang, Jiayin Li, Hui Zhang, Dan Zhao, Bingzheng Wei, and Yan Xu. 2024. Restore-RWKV: Efficient and Effective Medical Image Restoration with RWKV. CoRR abs/2407.11087 (2024).
- [54] Xumin Yu, Yongming Rao, Ziyi Wang, Zuyan Liu, Jiwen Lu, and Jie Zhou. 2021. PoinTr: Diverse Point Cloud Completion with Geometry-Aware Transformers.

- In ICCV. 12498-12507.
- [55] Xumin Yu, Yongming Rao, Ziyi Wang, Jiwen Lu, and Jie Zhou. 2023. AdaPoinTr: Diverse Point Cloud Completion with Adaptive Geometry-Aware Transformers. IEEE Transactions on Pattern Analysis and Machine Intelligence 45, 12 (2023).
- [56] Wentao Yuan, Tejas Khot, David Held, Christoph Mertz, and Martial Hebert. 2018. PCN: Point Completion Network. In 2018 International Conference on 3D Vision (3DV). IEEE, 728–737.
- [57] Jiahui Zhang, Hao Zhao, Anbang Yao, Yurong Chen, Li Zhang, and Hongen Liao. 2018. Efficient Semantic Scene Completion Network with Spatial Group Convolution. In ECCV. 733–749.
- [58] Shoulong Zhang, Shuai Li, Aimin Hao, and Hong Qin. 2021. Point Cloud Semantic Scene Completion from RGB-D Images. In AAAI, Vol. 35. 3385–3393.
- [59] Tao Zhang, Xiangtai Li, Haobo Yuan, Shunping Ji, and Shuicheng Yan. 2024. Point could mamba: Point cloud learning via state space model. arXiv preprint arXiv:2403.00762 (2024).
- [60] Hengshuang Zhao, Li Jiang, Jiaya Jia, Philip HS Torr, and Vladlen Koltun. 2021. Point Transformer. In ICCV. 16259–16268.
- [61] Haoran Zhou, Yun Cao, Wenqing Chu, Junwei Zhu, Tong Lu, Ying Tai, and Chengjie Wang. 2022. Seedformer: Patch seeds based point cloud completion with upsample transformer. In European conference on computer vision. Springer, 416–432.
- [62] Daoming Zong, Shiliang Sun, and Jing Zhao. 2021. ASHF-Net: Adaptive Sampling and Hierarchical Folding Network for Robust Point Cloud Completion. In AAAI, Vol. 35. 3625–3632.